BIOCHEMISTRY

Thanatin targets the intermembrane protein complex required for lipopolysaccharide transport in *Escherichia coli*

Stefan U. Vetterli[1], Katja Zerbe[1], Maik Müller[2], Matthias Urfer[1], Milon Mondal[1], Shuang-Yan Wang[1], Kerstin Moehle[1], Oliver Zerbe[1], Alessandra Vitale[3], Gabriella Pessi[3], Leo Eberl[3], Bernd Wollscheid[2], John A. Robinson[1]*

With the increasing resistance of many Gram-negative bacteria to existing classes of antibiotics, identifying new paradigms in antimicrobial discovery is an important research priority. Of special interest are the proteins required for the biogenesis of the asymmetric Gram-negative bacterial outer membrane (OM). Seven Lpt proteins (LptA to LptG) associate in most Gram-negative bacteria to form a macromolecular complex spanning the entire envelope, which transports lipopolysaccharide (LPS) molecules from their site of assembly at the inner membrane to the cell surface, powered by adenosine 5′-triphosphate hydrolysis in the cytoplasm. The periplasmic protein LptA comprises the protein bridge across the periplasm, which connects $LptB_2FGC$ at the inner membrane to LptD/E anchored in the OM. We show here that the naturally occurring, insect-derived antimicrobial peptide thanatin targets LptA and LptD in the network of periplasmic protein-protein interactions required to assemble the Lpt complex, leading to the inhibition of LPS transport and OM biogenesis in *Escherichia coli*.

INTRODUCTION

The asymmetric outer membrane (OM) plays a critical role in protecting Gram-negative bacteria from extracellular cytotoxic molecules, including antibiotics. This unique bilayer comprises lipopolysaccharide (LPS) molecules in the outer leaflet and membrane glycerophospholipids in the inner leaflet. Integral OM proteins (OMPs) are crucial for the biogenesis of the OM, as well as for controlling the uptake and export of essential nutrients and signaling molecules across the OM. Of special interest are the seven proteins (LptA to LptG) needed to transport LPS molecules from their site of assembly at the inner membrane (IM), across the aqueous periplasm, to their final cell surface location during OM biogenesis (*1*–*3*). The LptA to LptG proteins associate to form a macromolecular complex that spans the entire envelope (*4*, *5*). The periplasmic protein LptA, likely as a head-to-tail oligomer, forms a protein bridge spanning the periplasm. LPS molecules are pushed across this bridge (*6*–*10*), from $LptB_2FGC$ anchored in the IM to the LptDE complex embedded in the OM (Fig. 1A) (*11*–*16*), powered by adenosine 5′-triphosphate (ATP) hydrolysis in the cytoplasm (*4*). We report here that the naturally occurring, insect-derived host-defense peptide thanatin (Fig. 1B) targets both LptA and LptD in *Escherichia coli*.

Thanatin was first isolated from the hemipteran insect *Podisus maculiventris* (spined soldier bug) in 1996 (*17*). The peptide contains 21 amino acids (GSKKPVPIIYCNRRTGKCQRM) with a disulfide bond between Cys^{11} and Cys^{18}. Antimicrobial activity for thanatin was reported against *E. coli*, *Salmonella typhimurium*, *Klebsiella pneumoniae*, and *Enterobacter cloacae* with minimal inhibitory concentrations (MICs) of <1.5 μM and with weaker activity against *Erwinia carotovora* and *Pseudomonas aeruginosa* (MICs of 10 to 12 μM). Although no activity was seen against *Staphylococcus aureus*, thanatin is active against some other Gram-positive bacteria with MICs of ≈1 to 5 μM. Of special interest is the observation that the enantiomeric form (D-thanatin) loses much of its activity against all the Gram-negative strains tested, indicating a likely chiral target.

RESULTS

Mechanism of action

The mechanism of action of thanatin is so far unknown. The peptide is bactericidal against *E. coli*, shows only weak permeabilizing effects on the IM or OM, and does not cause hemolysis of blood erythrocytes even at 100× the MIC (*17*–*20*). We confirmed that thanatin has no membrane-permeabilizing effects on *E. coli*. The fluorescent dye SYTOX Green does not penetrate *E. coli* cells treated with thanatin even at 100 μg/ml (see section S3). Moreover, no release into the external medium of ß-lactamase expressed in the periplasm or of ß-galactosidase expressed in the cytoplasm of *E. coli* could be detected upon exposure to thanatin (see Supplementary Materials). Thus, even at concentrations much higher than the MIC, neither the IM nor the OM of *E. coli* is permeabilized by treatment with thanatin, unlike what is seen with some other cationic antimicrobial peptides, such as polymyxin B, colistin, or protegrin I (*21*, *22*).

The effects of thanatin on macromolecule biosynthesis were examined by monitoring the incorporation of appropriate [^{3}H]-labeled precursors into macromolecules in *E. coli* American Type Culture Collection (ATCC) 25922 (see section S4). No inhibition of protein, RNA, DNA, or cell wall biosynthesis was observed. To analyze effects on morphology, we grew *E. coli* cells with thanatin at concentrations causing substantial growth inhibition and then examined them in thin sections by transmission electron microscopy (TEM). This revealed frequent defects in membrane architecture, with accumulations of membrane-like material inside cells (Fig. 2, A and B). These multilayered membrane folds inside the cell are typical of those reported for *E. coli* in which LPS transport is inhibited by

[1]Chemistry Department, University of Zurich, Winterthurerstrasse 190, 8057 Zurich, Switzerland. [2]Institute of Molecular Systems Biology and Department of Health Sciences and Technology, ETH Zürich, Otto-Stern-Weg 3, 8093 Zürich, Switzerland. [3]Department of Plant and Microbial Biology, University of Zurich, Zollikerstrasse 107, 8008 Zurich, Switzerland.
*Corresponding author. Email: john.robinson@chem.uzh.ch

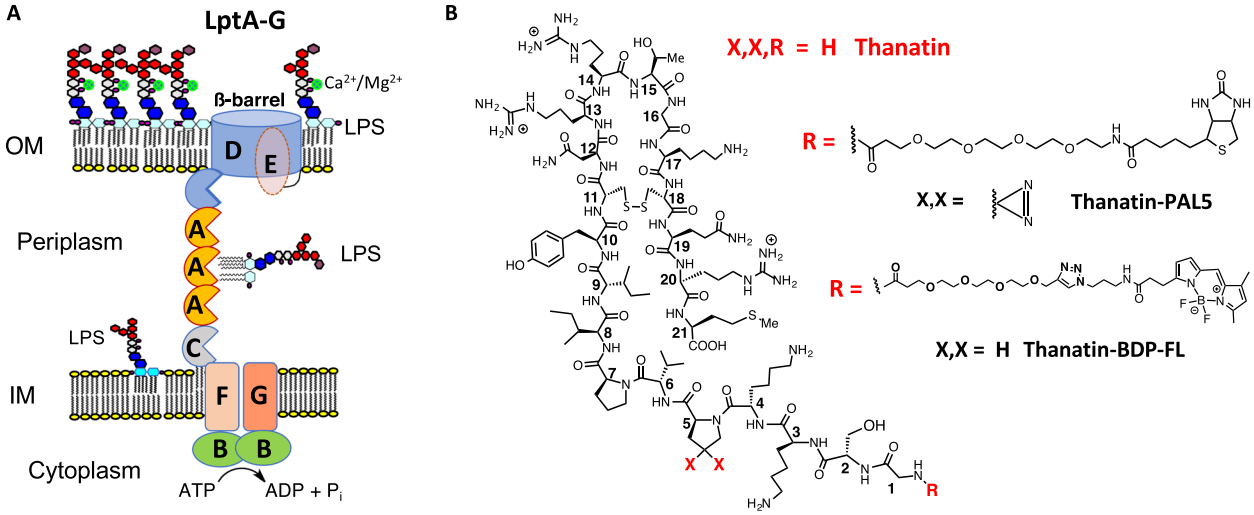

Fig. 1. LPS transport pathway and thanatin-based probes. (**A**) The LPS transport apparatus in Gram-negative bacteria comprises the seven proteins LptA to LptG, which form a macromolecular complex spanning the IM and OM. LPS transport across the periplasm occurs over a bridge formed by one or more copies of LptA. ADP, adenosine 5′-diphosphate. (**B**) Structures of thanatin and the photoprobe thanatin-PAL5 and fluorescence probe thanatin-BDP-FL.

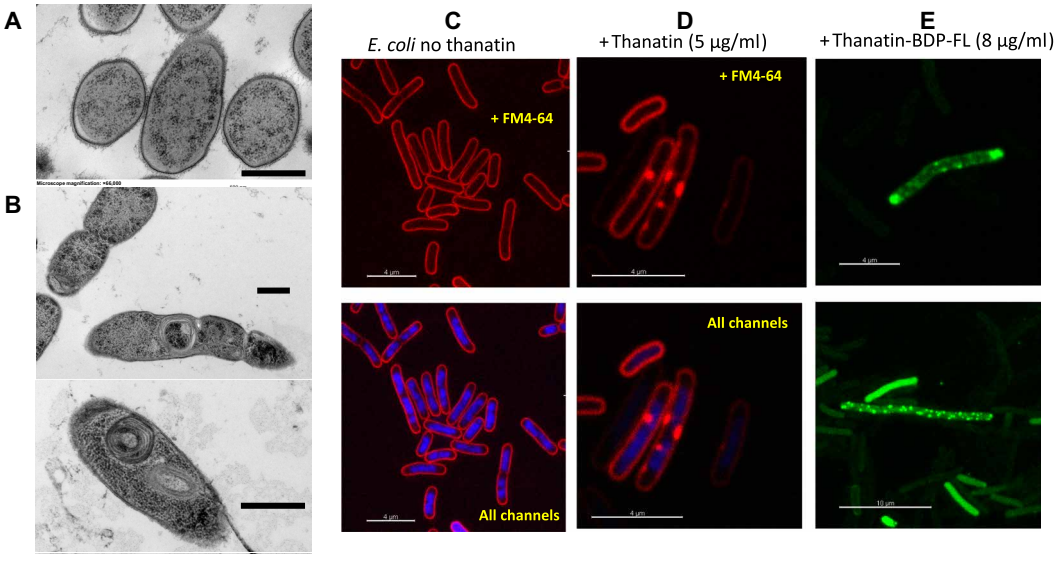

Fig. 2. Electron and fluorescence microscopy studies. (**A** and **B**) TEM studies of *E. coli* ATCC 25922, before (A) and after (B) thanatin treatment (1.5 µg/ml), showing internal accumulations of membrane-like material. Scale bars, 500 nm. (**C** and **D**) Super-resolution fluorescence microscopy of *E. coli* ATCC 25922 without (C) or with thanatin (5 µg/ml) (D) and stained with FM4-64, SYTOX Green, or DAPI. Top: The FM4-64 channel (red staining). Bottom: Superimposition of all three channels [with DAPI (blue) and SYTOX Green (nondetected)]. (**E**) *E. coli* staining with thanatin-BDP-FL (8 µg/ml) for 2 hours at 30°C (both pictures). Cells were analyzed using a Leica CLSM SP8 gSTED microscope. Scale bars, 4 or 10 µm (bottom right). For experimental details, see section S5.

down-regulation of LptA/B, LptC, or LptD (*5*, *16*). The effects of thanatin on *E. coli* were also monitored by laser scanning stimulated emission depletion (STED) fluorescence microscopy, with staining of membranes by the membrane dye FM4-64, of nucleoids by 4′,6-diamidino-2-phenylindole (DAPI), and using SYTOX Green to detect permeabilized cells (Fig. 2, C and D). These studies revealed frequent accumulations of membrane-like material in the form of knobs stained bright red by FM4-64 and elongated cell assemblies, with neither effect visible in the absence of thanatin. Nucleoids stained with DAPI were not influenced significantly by thanatin, and again no significant staining was observed by SYTOX Green. These results reveal that thanatin causes defects in the membrane assembly in *E. coli*.

A fluorescent derivative (thanatin-BDP-FL; MIC of ≈1 to 2 µg/ml; Fig. 1B) was used for STED fluorescence imaging. This probe stained the *E. coli* envelope, with marked focal accumulations (as green fluorescent knobs) across the cell and at the cell poles (Fig. 2E). This behavior is reminiscent of fluorescent labeling of OMPs that accumulate into membrane islands or clusters and at the poles in Gram-negative bacteria (*23*, *24*). The interaction of thanatin with OMPs in *E. coli* was tested directly by photoaffinity labeling experiments. Two thanatin-derived photoprobes were synthesized

containing photoproline (*25*, *26*), in place of either Pro^5 or Pro^7, together with an N-terminal polyethylene glycol linker and biotin tag for pull-down assays (Fig. 1B and sections S2 and S5). Both probes (thanatin-PAL5 and thanatin-PAL7) maintained antimicrobial activity against *E. coli* ATCC 25922 (MICs of 2 to 4 μg/ml) and photolabeled the same membrane proteins in vivo, as shown in Western blotting for thanatin-PAL5 in Fig. 3A. In a competitive photolabeling experiment with native thanatin (200 μg/ml) as a competitor, thanatin-PAL5 (2 μg/ml) labeling of the ≈95-kDa band largely disappeared from the blot, whereas the other signals showed reduced labeling (Fig. 3A). When the in vivo photolabeled membrane protein extract was analyzed under nonreducing conditions to retain disulfide bonds, a shift of the ≈95-kDa band to ≈130 kDa was seen in the Western blot (Fig. 3B and the Supplementary Materials). This change in gel electrophoretic mobility is very characteristic of that reported for *E. coli* LptD in the disulfide-reduced and disulfide-oxidized forms ($LptD_{ox}$ ≈ 130 kDa and $LptD_{red}$ ≈ 90 kDa) (*27*, *28*).

It was technically not possible to identify photolabeled proteins directly from the Western blots. To identify thanatin interaction partners in a hypothesis-free, discovery-driven approach, we used the photoaffinity interaction mapping strategy outlined above, in combination with mass spectrometry (MS)–based proteomic analysis, which allows for the multiplexed and label-free quantification of *E. coli* interaction partners. Thanatin-PAL5–photolabeled and untreated control *E. coli* ATCC 25922 cells were lysed, and biotinylated proteins were purified using streptavidin-functionalized agarose resin. Enriched proteins were proteolytically digested and subsequently identified using high-performance liquid chromatography–tandem MS (HPLC-MS/MS). Four hundred proteins were identified at a false discovery rate (FDR) below 1%. Relative quantitative comparison revealed the specific and photolabeling-dependent enrichment of three proteins, namely, LptD, LptA, and BamB, of which LptD and LptA were the most significant (Fig. 3C). Whereas photolabeling of the membrane protein LptD was already suggested by the Western blotting experiments described above, photolabeling of LptA, a small (≈18 kDa) soluble periplasmic component of the LPS transport pathway (Fig. 1A), was unexpected.

Resistant mutants

Spontaneous thanatin-resistant ($Than^R$) mutants of *E. coli* ATCC 25922 were sought for genetic analysis. $Than^R$ mutants could be isolated at low frequency (≈1 in 10^8 colony-forming units (CFU); 10^{-6}%) by passaging on Mueller-Hinton II (MH-II) agar containing thanatin (10 to 50 μg/ml). Five $Than^R$ mutants were selected that remained stable over at least four passages on thanatin-free agar (see section S6). Three mutants showed no difference in growth behavior compared to the wild-type (WT) in MH-II media and no increased sensitivity on MH-II agar supplemented with 0.5% SDS and 1 mM EDTA. Also, the susceptibility of all mutants to a series of standard antibiotics was unchanged (see section S6). Whole-genome sequencing of the three $Than^R$ mutants revealed several mutations compared to the WT genome, including *lptA* as the only mutated gene common to all three. Moreover, one resistant mutant ($Than^R$-8) contained only a single point mutation in the entire genome, corresponding to a change of glutamine to leucine at position 62 (Q62L) in LptA. We also tested whether the identified mutations Q62L-LptA and D31N-LptA would confer resistance to thanatin when introduced into a sensitive *E. coli* strain. For this, genes encoding

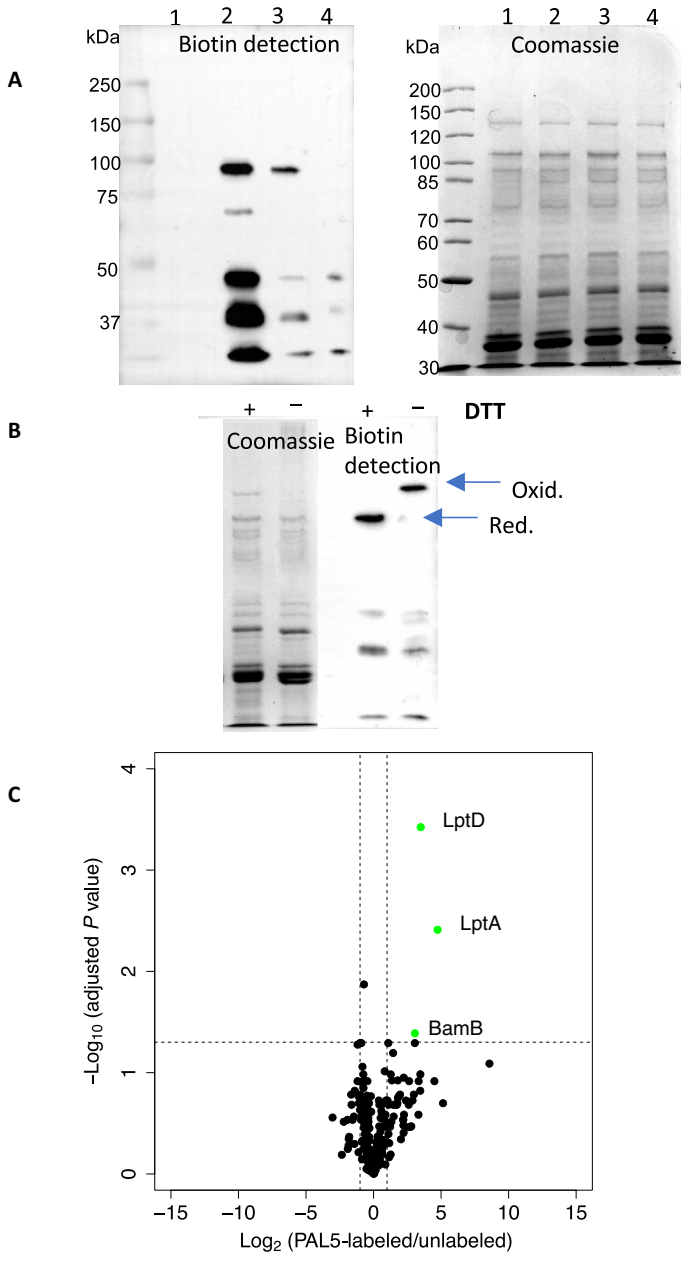

Fig. 3. Photolabeling of *E. coli* ATCC 25922 with thanatin-PAL5. (**A**) Western blot (biotin detection) and corresponding SDS–polyacrylamide gel electrophoresis (SDS-PAGE) (Coomassie blue staining) of membrane protein fraction from: lane 1, control unlabeled cells; lanes 2 and 3, cells photolabeled with thanatin-PAL5 (10 and 2 μg/ml); and lane 4, cells photolabeled with thanatin-PAL5 (10 μg/ml) + competitor thanatin (200 μg/ml). (**B**) Western blot and SDS-PAGE after photolabeling with thanatin-PAL5 (2 μg/ml) with (+) or without (–) reduction of extracted membrane proteins with dithiothreitol (DTT). (**C**) Volcano plot showing relative abundance of *E. coli* proteins in thanatin-PAL5 labeled versus unlabeled control sample after streptavidin pulldown detected by MS-based proteomic analysis. Significantly enriched proteins (right/above dashed lines) are highlighted in green and represent PAL5-labeled proteins.

LptA with a His6 tag at the C terminus (LptA-His6), as well as the corresponding mutated variants (Q62L-LptA-His6 and D31N-LptA-His6), were introduced into *E. coli*. Introduction of the mutant alleles led to a markedly higher MIC for thanatin, whereas introduction of

the WT sequence (LptA-His6) gave no significant change in MIC (see section S6). In summary, the genetic and photolabeling results reveal a link between the antimicrobial activity of thanatin and LptA and point to LptA as an interaction partner for thanatin in *E. coli*. On the other hand, no mutations in *lptD* were detected in the genomes of the three analyzed Than^R mutants.

In vitro binding studies

To date, no small molecules (apart from LPS) are known to interact with LptA, so we tested whether thanatin can directly bind to LptA in vitro. A recombinant full-length LptA [with a His6 tag fused to the C terminus (LptA-His6)] was produced in *E. coli* BL21(DE3) and purified to apparent homogeneity by SDS-PAGE after Ni–nitrilotriacetic acid affinity and anion exchange chromatography (see section S7). The binding of thanatin-BDP-FL (Fig. 1B) to LptA-His6 was then studied by fluorescence polarization (FP) and of thanatin binding to LptA labeled with DyLight650 by thermophoresis. Using both biophysical methods, fitting the binding isotherm to a 1:1 Langmuir binding model (see section S8) gave by FP a dissociation constant (K_d) of 12 ± 3 nM and by thermophoresis a K_d of 20 ± 1 nM. In control experiments using the enantiomeric form of thanatin (comprising all D-amino acids), no interaction of D-thanatin with LptA was observed by FP. The binding of thanatin to LptD was also measured in vitro using a recombinant His-tagged LptD/E complex purified from *E. coli* (see section S7.2). Using FP, thanatin-BDP-FL binds to LptD/E$_{His}$ with a K_d of 34 ± 5 nM, whereas thermophoresis binding assays gave a K_d of 44 ± 27 nM (see section S9). Thanatin therefore binds in vitro to both LptA and LptD/E in the low nanomolar range.

Nuclear magnetic resonance structural studies

To characterize the epitope on LptA involved in binding to thanatin, complex formation was monitored by [^{15}N,^{1}H]–heteronuclear single-quantum coherence (HSQC) nuclear magnetic resonance (NMR) spectroscopy using a recently described, nonaggregating, truncated derivative of LptA called LptA$_m$, lacking the last C-terminal ß-strand (*10*). We confirmed in vitro that thanatin binds with the same high affinity also to LptA$_m$ (see section S8). Therefore, the lack of the last C-terminal ß-strand in this LptA$_m$ construct, which is important to prevent unwanted aggregation, does not affect binding to thanatin. This result is understandable, as we show later that thanatin interacts with the N-terminal ß-strands of LptA (vide infra). [^{15}N,^{1}H]-HSQC spectra revealed complete and stable complex formation in the slow-exchange regime on the NMR time scale upon addition of thanatin to [^{15}N]-LptA$_m$ to a ca. 1:1.2 molar ratio (see section S10). Free LptA$_m$ and the complex of LptA$_m$ with thanatin displayed a high-quality [^{15}N,^{1}H]-HSQC spectrum with good signal dispersion, indicating that the protein-peptide complex was well folded and probably rich in β sheet. While many ^{1}H-^{15}N correlations in [^{15}N]-LptA$_m$ were unchanged upon thanatin binding, a multitude of other cross-peaks showed significant chemical shift perturbations (see section S10). The structure of the thanatin-LptA$_m$ complex (Fig. 4A) was then determined by multidimensional NMR methods using mixtures of unlabeled and [^{13}C,^{15}N]-labeled forms of thanatin and LptA$_m$ in isotope-edited/filtered nuclear Overhauser effect spectroscopy (NOESY) experiments.

In the complex, the N-terminal strand of the thanatin ß-hairpin (Pro^7-Asn^{12}) docks in a parallel orientation onto the first (N-terminal) ß-strand in the ß-jellyroll of LptA$_m$ (Pro^{35}-Ser^{40}), with the strand orientation being defined by multiple interstrand NOEs (Fig. 4B). Following the ß-turn in thanatin (Arg^{13}-Gly^{16}), the C-terminal strand (Lys^{17}-Met^{21}) is mostly solvent exposed (Fig. 4, A to C), although the side chain of Met^{21} nestles into a hydrophobic site on the surface of LptA$_m$. Hydrophobic residues on the thanatin N-terminal ß-strand, particularly Ile^8 and Tyr^{10}, are buried in the hydrophobic interior of the ß-jellyroll (Fig. 4A), in a cavity formed by LptA$_m$ side chains Ile^{38}, Leu^{45}, Val^{52}, Phe^{54}, Val^{74}, and Ile^{86}, as evidenced by a network of NOEs seen in NOESY spectra. It seems likely that multiple van der Waals contacts and a π-π stacking interaction (Than.Tyr^{10}-LptA$_m$.Phe^{54}) made between these residues may help to stabilize the complex. Moreover, aliphatic residues of thanatin (Val^6 and Pro^7) pack against Pro^{35} and Ile^{36} near to the N terminus of LptA$_m$, thereby forming another hydrophobic interaction, which helps to establish the orientation of the N-terminal part of thanatin. This interaction affects the orientation of the short N-terminal helix in LptA$_m$, including Asp^{31}, which in turn packs against a loop of the ß-jellyroll containing Gln^{62} (Fig. 4C). This proximity might explain why mutations at Asp^{31}/Gln^{62} in LptA have a strong influence upon thanatin binding (vide supra). In addition, the N terminus of thanatin displays NOE contacts with residues from the loop of the opposite side of the ß-jellyroll (Gly^{78}-Gly^{82}). This loop is missing in the x-ray structure of free LptA (*9*), likely because of its flexibility. Last, the side chains of thanatin Asn^{12} and Arg^{13} are likely involved in hydrogen bonding and formation of electrostatic interactions with LptA$_m$, respectively. The amide side-chain protons of Asn^{12}, whose resonances are significantly downfield shifted in complex with LptA$_m$, are in a suitable geometry to form hydrogen bonds with the backbone carbonyl oxygen atoms of Ser^{40} and Asp^{41}. The guanidinium groups of Arg^{13} and Arg^{14} in thanatin are within salt bridge distances to carboxylate groups in LptA$_m$ (Than.Arg^{13}-LptA$_m$.Glu^{39} and Than.Arg^{14}-LptA$_m$.Asp^{41}).

DISCUSSION

It has been shown that LptA can form head-to-tail homodimers in vivo, although it remains possible that a single LptA molecule can bridge the periplasm by contacting both LptC and N-LptD (Fig. 1) (*7*). Furthermore, the known crystal structure of an LptA head-to-tail oligomer [Protein Data Bank (PDB) 2R1A] reveals the N-terminal ß-strands of one subunit interacting with the C-terminal strands of the next LptA subunit (*9*). This interaction is likely important in assembling the LptA protein bridge across the periplasm in the macromolecular Lpt complex (Fig. 1A). In addition, the N-terminal strands of LptA mediate the binding of LptA to the membrane-anchored LptC (Fig. 1) (*7*, *9*, *29*, *30*). The NMR structure of LptA complexed with thanatin, reported here, superimposed upon the crystal structure of the LptA head-to-tail oligomer (PDB 2R1A), reveals that the thanatin binding site overlaps and would therefore block the interaction between LptA subunits (Fig. 4D). It also seems likely that thanatin will inhibit the LptA/C protein-protein interaction. Last, the C-terminal strands of LptA bind to the N-terminal ß-strands in the periplasmic ß-jellyroll domain of LptD. It is intriguing that the structure of the N-terminal ß-strands of the ß-jellyroll in LptD is highly similar to those in LptA (*14*, *15*). Residues in LptA that contact thanatin in the complex are highly conserved in the same positions in LptD (see section S10 and fig. S12). This strongly suggests that thanatin should interact with the N-terminal ß-strands in the ß-jellyroll of LptD/E. This implies that thanatin should also inhibit the interaction of LptA with LptD. Reported affinities of the LptA-LptA

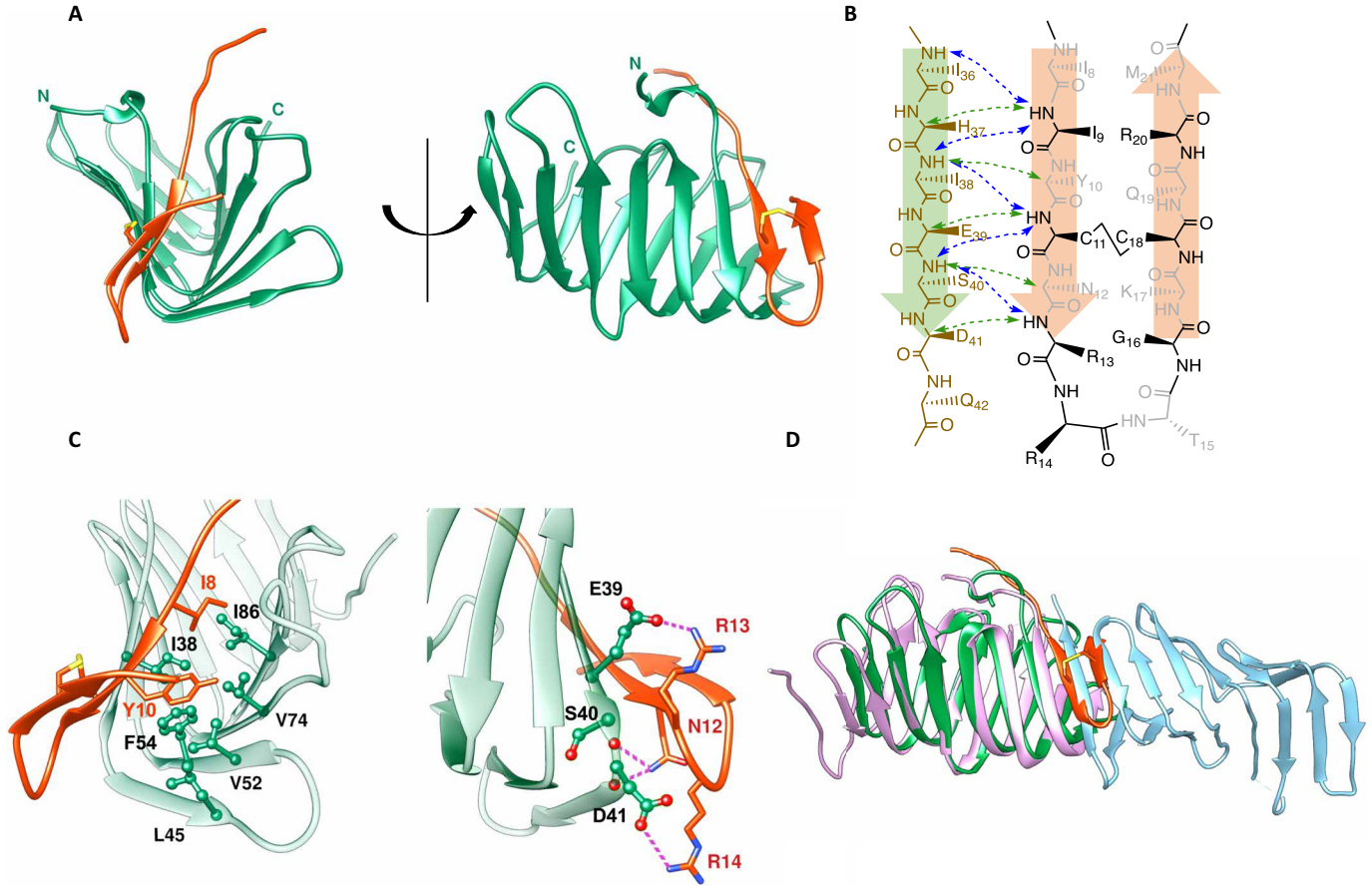

Fig. 4. The solution structure of the LptA$_m$-thanatin complex. (**A**) Ribbon representation of a single NMR LptA$_m$-thanatin complex in two different orientations. LptA$_m$ and thanatin are in green and orange, respectively. The flexible C terminus of LptA$_m$ encompassing residues 144 to 159 and the His tag are not shown. (**B**) Structurally relevant intermolecular NOEs between backbone atoms of the first β-strands of LptA and thanatin are indicated with dashed arrows, and H^N-H^N and H^N-Hα NOEs are colored in blue and green, respectively. (**C**) Ribbon model of the LptA$_m$-thanatin complex. Residues involved in the protein-peptide hydrophobic interface (left) and in hydrogen bonding and electrostatic interactions (right) are indicated by ball-and-stick representation. (**D**) Superposition of the LptA dimer (PDB 2R1A; chains B (light blue) and C (violet) with the LptA$_m$-thanatin complex (green/orange). Thanatin occupies a binding site on LptA$_m$ which is used to mediate LptA-LptA interactions needed to form the periplasmic bridge connecting IM and OM for LPS transport.

and LptA-LptC interactions have K_ds in the low micromolar range (*8*, *31*). The nanomolar affinity of thanatin to both LptA and LptD reported here, therefore, appears strong enough to inhibit multiple protein-protein interactions required for the assembly of the LPS trans-periplasmic protein complex.

These results highlight a new paradigm for an antibiotic action, targeting a dynamic network of protein-protein interactions required for assembly of the Lpt complex in *E. coli*. The results also identify one naturally occurring peptide as a starting point for the development of potential clinical candidates that target dangerous Gram-negative bacterial pathogens. Last, this work may also contribute to a better understanding of the biological function of thanatin in its natural context: controlling titers of symbiotic or invading bacterial pathogens in the midgut of various insect species (*32*).

MATERIALS AND METHODS

Peptide synthesis

Methods of synthesis and analytical data for all peptides are included in the Supplementary Materials.

Methods for fluorescence and electron microscopy

Methods for fluorescence microscopy and TEM have been described in detail previously (*24*).

Photoaffinity labeling

E. coli ATCC 25922 cells grown in MH-I broth (50 ml) to an OD_{600} (optical density at 600 nm) of 1.0 were collected, washed once, taken up in phosphate-buffered saline (PBS) (50 ml), and incubated for 30 min at 37°C with shaking at 200 rpm in the dark with thanatin-PAL5 (2 to 10 μg/ml). Photoactivation was achieved by ultraviolet irradiation at 350 nm in a Rayonet Reactor (16 × 8-W Sylvania blacklight lamps) for 30 min at 30°C. Cells were then collected and washed two times with PBS. Cell pellets can be stored at −20°C. The cell pellet was resuspended in 50 mM tris-HCl (pH 7.3) with protease inhibitor cocktail (cOmplete, Roche) and lysed by three cycles of sonication using a Branson Digital Sonifier equipped with a microtip (80 W, 30% intensity, 20 s on, with 20 s off for 2 min) under cooling on ice. To remove unbroken cells and cell debris, the lysate was centrifuged (30 min at 4000 rpm, 4°C). The supernatant was subjected to ultracentrifugation (200,000*g*, in a Sorvall T-875 rotor for 1 hour, 4°C). The pellet was washed with

50 mM tris-HCl (pH 7.3) and collected again by ultracentrifugation (1 hour, 4°C).

Identification of photolabeled proteins by MS

Photolabeled and PBS-washed *E. coli* were lysed in 50 mM ammonium bicarbonate (AmBic) containing protease inhibitor cocktail (catalog no. 11704900, Roche) and 0.1% RapiGest (catalog no. 186002122, Waters) by six intervals of 30-s ultrasound sonication in a vial tweeter (Hielscher Ultrasonics GmbH) at a power of 170 W and 80% cycle time. Protein concentration was determined by a NanoDrop 2000 Spectrophotometer (Thermo Fisher Scientific Inc.), and 10 mg of protein was incubated with 200 µl of streptavidin agarose resin (catalog no. 53116, Thermo Fisher Scientific) for 100 min at 4°C to bind biotinylated proteins. Beads were settled by centrifugation at 2000*g* for 5 min and transferred to Mobicol columns equipped with a 30-µm pore size filter (MoBiTec GmbH). Beads were extensively washed with 5 M NaCl, StimLys buffer [50 mM tris (pH 7.8), 137 mM NaCl, 150 mM glycerol, 0.5 mM EDTA, 0.1% Triton X-100], 100 mM $NaHCO_3$, and AmBic to remove nonbiotinylated proteins. Bead-bound proteins were reduced with 5 mM tris(2-carboxyethyl) phosphine in AmBic for 40 min at 37°C, alkylated with 10 mM iodoacetamide in AmBic for 30 min at 37°C, and proteolytically digested by sequencing-grade modified trypsin (catalog no. V511A, Promega) at an enzyme-to-protein ratio of 1:100 for 20 hours at 37°C. Released peptides were acidified and subjected to C18 purification using UltraMicroSpin Columns (The Nest Group).

Peptide samples were separated by reversed-phase chromatography on an HPLC column (75-µm inner diameter, New Objective) that was packed in-house with a 15-cm stationary phase (ReproSil-Pur C18-AQ, 1.9 µm) and connected to a nanoflow HPLC with an autosampler (EASY-nLC 1000, Thermo Fisher Scientific). The HPLC was coupled to a Q Exactive Plus mass spectrometer (Thermo Fisher Scientific) equipped with a nanoelectrospray ion source (Thermo Fisher Scientific). Peptides were loaded onto the column with 100% buffer A [99.9% H_2O, 0.1% formic acid (FA)] and eluted at a constant flow rate of 300 nl/min with a 30-min linear gradient from 6 to 20% buffer B (99.9% MeCN and 0.1% FA) followed by a 15-min transition from 20 to 32% buffer B. Electrospray voltage was set to 2 kV, sheath and auxiliary gas flow to zero, and capillary temperature to 250°C. In data-dependent acquisition (DDA) mode, the mass spectrometer automatically switched between precursor and fragment ion detection. Following a high-resolution survey mass spectrum [from 300 to 1500 mass/charge ratio (m/z)] acquired in the Orbitrap with resolution R = 70,000 at m/z 200 (automatic gain control target value 3×10^6), the 15 most abundant peptide ions with a minimum intensity of 2.5×10^4 were selected for subsequent higher-energy collisional dissociation fragmentation with an isolation window of 1.4 Da, and fragments were detected by MS/MS acquisition in the Orbitrap at resolution R = 35,000 (automatic gain control target value of 1×10^6). Target ions already selected for fragmentation were dynamically excluded for 30 s.

Acquired raw files were subjected to protein identification using Comet (v.2015.01) and Trans Proteomic Pipeline v.4.7 (Seattle Proteome Center/Institute of Systems Biology, Seattle) by matching ion spectra acquired in the DDA mode against a SwissProt (UniProt consortium)–reviewed *E. coli* protein database (downloaded November 2016). Peptides were required to be fully tryptic with a maximum of two missed cleavage sites, carbamidomethylation as a fixed modification and methionine oxidation as a dynamic modification. The precursor and fragment mass tolerance were set to 20 parts per million (ppm) and 0.02 Da, respectively. Identified proteins were quantified by integration of chromatographic traces of peptides using Progenesis QI v.2.0 (Nonlinear Dynamics, UK). Contaminant hits were removed, and proteins were filtered to obtain an FDR of <1%. Raw protein abundances based on nonconflicting peptides were exported, and differential abundance testing was performed using R package MSstats v3.5.3 (*33*). Significantly enriched *E. coli* proteins (abundance fold change ≥ 2 and adjusted P values of ≤0.05) were considered as bona fide thanatin-PAL5–binding candidates. Mass spectrometric data were deposited to the ProteomeXchange Consortium (www.proteomexchange.org/) via the PRIDE partner repository (data set identifier: PXD010988).

Thanatin-resistant *E. coli* mutants

E. coli ATCC 25922 was grown in MH-II broth (20 ml) to OD_{600nm} = 1 at 37°C with 200 rpm shaking. This bacterial culture (100 µl, corresponding to $\approx 5 \times 10^7$ CFU) was plated onto MH-II agar plates containing thanatin (10 to 50 µg/ml) and incubated at 37°C overnight. Growing colonies were then passaged at least four times over MH-II plates without selection on thanatin, and then MIC values against thanatin were determined. Two independent experiments were performed. Of the initial 10 isolates, the mutants $Than^R$-2, $Than^R$-4, $Than^R$-8, $Than^R$-9, and $Than^R$-10 exhibited stable resistance (MIC of ≥64 µg/ml), and, in each, the *lptA* gene was sequenced, which revealed mutations Q62L or D31N in the primary sequence of the protein (table S2). The antimicrobial activity of thanatin and seven standard antibiotics against the three selected mutants ($Than^R$-2, $Than^R$-4, and $Than^R$-8) are shown in table S3.

The complete genomes of three selected mutants ($Than^R$-2, $Than^R$-4, and $Than^R$-8) and the WT (ATCC 25922) strain used in these studies were sequenced using the Illumina MiSeq platform (MiSeq Reagent Kit V2; 500 cycles). Briefly, genomic DNA (gDNA) of the WT and the selected mutants was extracted using the Sigma NA2100 1Kit. One microgram of gDNA was sheared to 500 base pairs by sonication (Covaris). DNA fragments were further processed with the NEBNext Ultra II DNA Library Prep Kit for Illumina (NEB #E7645S/L). Genome mapping and identification of genetic variants were performed using CLC Genomics Workbench 10.1.1 (CLC bio). The genes mutated in the resistant strains, compared to the WT, are shown in table S4. In the $Than^R$-8 resistant strain, only a single base pair change was found in the entire genome, in the *lptA* gene, corresponding to a Q62L change in the primary sequence of the protein.

Binding and NMR studies and structure determination of thanatin-$LptA_m$ complex

Production of LptA-His6, $LptA_m$, LptD/E, and thanatin in *E. coli* and details of binding assays with LptA by FP and thermophoresis are described in sections S7 to S9. Production of [^{15}N]- and [^{15}N,^{13}C]-labeled $LptA_m$ was performed in BL21(DE3) *E. coli* cells grown in M9 minimal medium appropriately supplemented with $^{15}NH_4Cl$ and ^{13}C glucose at 25°C overnight. Purification is described in section S7. The addition of 20 mM CHAPS to the sample buffer significantly improved the quality of the [^{15}N,^{1}H]-HSQC spectra by reducing line-broadening effects due to aggregation (see figs. S8 and S9). Final NMR samples contained 50 mM sodium phosphate, 150 mM NaCl (pH 7.5), and protein/peptide concentrations of 0.5 to 0.6 mM.

NMR spectra were acquired at 290 K (free ^{15}N-thanatin) and at 308 K (free ^{15}N,^{13}C LptA$_m$, and complex of LptA$_m$-thanatin) using 700- and 600-MHz Bruker NEO spectrometers. All spectra were processed using TopSpin 4.0 and analyzed using CARA and CCPNmr. The ^{1}H, ^{15}N, and ^{13}C chemical shifts of backbone and side-chain atoms were assigned using a standard set of triple-resonance experiments on either uniformly ^{15}N,^{13}C-labeled LptA$_m$ with or without unlabeled thanatin or with uniformly ^{15}N,^{13}C-labeled thanatin with or without unlabeled LptA$_m$ at protein concentrations of 0.5 to 0.6 mM. The LptA$_m$-thanatin complex was prepared at a ratio of 1:1.2.

Backbone assignment was initiated from manually picked [^{15}N,^{1}H]-HSQC spectra that served as anchoring points for HNCO, HN(CO)CACB, and HNCACB experiments (*34*). Sequential resonance assignments used the standard strip matching procedure for Cα/Cβ chemical shifts. Backbone and side-chain chemical shift assignments were obtained for 89.7 and 85.7% of residues 28 to 143 of LptA$_m$ and 92.7 and 96.6% of residues 1 to 21 of thanatin, respectively. We noticed that resonances from the presumably unstructured C-terminal tail including the His tag (residues 144 to 170) and some residues in the longer loop regions (β6-β7) were often missing, likely because of accelerated amide proton exchange at pH 7.5. To this end, we adjusted the sample of the LptA-thanatin complex to pH 4.6 and remeasured the triple-resonance spectra. The overall signal dispersion in the [^{15}N,^{1}H]-HSQC spectra was not changed significantly, indicating a stable complex formation under those conditions. Additional amide cross peaks could be assigned to residues located in solvent-exposed loops or strands, namely, Gly^{30}, Gln^{43}, Met^{47}, Gly^{78}, Asp^{101}, and Asp^{139}. Many more peaks became visible that were often characterized by negative values of the ^{15}N{^{1}H}-NOEs, indicating that they belonged to flexible amide moieties but could not be assigned unambiguously.

Hβ and Hα chemical shifts obtained from the HBHA(CO)NH experiment were used in combination with Cα/Cβ chemical shifts from the backbone assignments to obtain side-chain assignments in HCCH experiments. The aromatic side chains were linked to the backbone using the (HB)CB(CGCDCD)HD and (HB)CB(CGCDCDCE)HE experiments (*35*). The assignment of thanatin resonances in the complex was performed in a similar manner. Proton chemical shifts were referenced to the water line at 4.65 ppm at 308 K, from which the nitrogen and carbon scales were derived indirectly by using the conversion factors of 0.10132900 (^{15}N) and 0.25144954 (^{13}C). All chemical shifts were deposited in the Biological Magnetic Resonance Data Bank (BMRB) database under ID 34261.

Upper-distance restraints used for the structure calculations of the LptA$_m$-thanatin complex were generated from 70-ms ^{15}N- and ^{13}C-NOESY (aliphatic and aromatic carbons) spectra. Intermolecular restraints were obtained from 70-ms ^{13}C,^{15}N-filtered/^{13}C-edited (aliphatic and aromatic ^{13}C), and ^{13}C,^{15}N-filtered/^{15}N-edited NOESY spectra, and all experiments were performed on two samples (^{13}C,^{15}N-labeled LptA$_m$/unlabeled thanatin and unlabeled LptA$_m$/^{13}C,^{15}N-labeled thanatin). Additional torsion angle restraints were derived from backbone chemical shifts using the program TALOS+ (*36*). The solution structure of the LptA$_m$-thanatin complex was determined using distance restraints derived from a set of NOESY spectra and torsion angle restraints derived from TALOS+. A full description of the structure calculations and statistical analysis of results is given in the Supplementary Materials.

SUPPLEMENTARY MATERIALS

Supplementary material for this article is available at http://advances.sciencemag.org/cgi/content/full/4/11/eaau2634/DC1

REFERENCES AND NOTES

1. A. Konovalova, D. E. Kahne, T. J. Silhavy, Outer membrane biogenesis. *Annu. Rev. Microbiol.* **71**, 539–556 (2017).
2. S. Okuda, E. Freinkman, D. Kahne, Cytoplasmic ATP hydrolysis powers transport of lipopolysaccharide across the periplasm in E. coli. *Science* **338**, 1214–1217 (2012).
3. S. Okuda, D. J. Sherman, T. J. Silhavy, N. Ruiz, D. Kahne, Lipopolysaccharide transport and assembly at the outer membrane: The PEZ model. *Nat. Rev. Microbiol.* **14**, 337–345 (2016).
4. D. J. Sherman, R. Xie, R. J. Taylor, A. H. George, S. Okuda, P. J. Foster, D. J. Needleman, D. Kahne, Lipopolysaccharide is transported to the cell surface by a membrane-to-membrane protein bridge. *Science* **359**, 798–801 (2018).
5. P. Sperandeo, F. K. Lau, A. Carpentieri, C. De Castro, A. Molinaro, G. Dehò, T. J. Silhavy, A. Polissi, Functional analysis of the protein machinery required for transport of lipopolysaccharide to the outer membrane of Escherichia coli. *J. Bacteriol.* **190**, 4460–4469 (2008).
6. A. X. Tran, M. S. Trent, C. Whitfield, The LptA protein of Escherichia coli is a periplasmic lipid-A-binding protein involved in the lipopolysaccharide export pathway. *J. Biol. Chem.* **283**, 20342–20349 (2008).
7. E. Freinkman, S. Okuda, N. Ruiz, D. Kahne, Regulated assembly of the transenvelope protein complex required for lipopolysaccharide export. *Biochemistry* **51**, 4800–4806 (2012).
8. J. A. Merten, K. M. Schultz, C. S. Klug, Concentration-dependent oligomerization and oligomeric arrangement of LptA. *Protein Sci.* **21**, 211–218 (2012).

9. M. D. L. Suits, P. Sperandeo, G. Dehò, A. Polissi, Z. Jia, Novel structure of the conserved Gram-negative lipopolysaccharide transport protein A and mutagenesis analysis. *J. Mol. Biol.* **380**, 476–488 (2008).
10. C. Laguri, P. Sperandeo, K. Pounot, I. Ayala, A. Silipo, C. M. Bougault, A. Molinaro, A. Polissi, J. P. Simorre, Interaction of lipopolysaccharides at intermolecular sites of the periplasmic Lpt transport assembly. *Sci. Rep.* **7**, 9715 (2017).
11. H. Dong, Z. Zhang, X. Tang, N. G. Paterson, C. Dong, Structural and functional insights into the lipopolysaccharide ABC transporter $LptB_2FG$. *Nat. Commun.* **8**, 222 (2017).
12. Q. S. Luo, X. Yang, S. Yu, H. Shi, K. Wang, L. Xiao, G. Zhu, C. Sun, T. Li, D. Li, X. Zhang, M. Zhou, Y. Huang, Structural basis for lipopolysaccharide extraction by ABC transporter $LptB_2FG$. *Nat. Struct. Mol. Biol.* **24**, 469–474 (2017).
13. I. Botos, N. Majdalani, S. J. Mayclin, J. G. McCarthy, K. Lundquist, D. Wojtowicz, T. J. Barnard, J. C. Gumbart, S. K. Buchanan, Structural and functional characterization of the LPS transporter LptDE from gram-negative pathogens. *Structure* **24**, 965–976 (2016).
14. H. Dong, Q. Xiang, Y. Gu, Z. Wang, N. G. Paterson, P. J. Stansfeld, C. He, Y. Zhang, W. Wang, C. Dong, Structural basis for outer membrane lipopolysaccharide insertion. *Nature* **511**, 52–56 (2014).
15. S. Qiao, Q. Luo, Y. Zhao, X. J. Zhang, Y. Huang, Structural basis for lipopolysaccharide insertion in the bacterial outer membrane. *Nature* **511**, 108–111 (2014).
16. T. Wu, A. C. McCandlish, L. S. Gronenberg, S.-S. Chng, T. J. Silhavy, D. Kahne, Identification of a protein complex that assembles lipopolysaccharide in the outer membrane of *Escherichia coli*. *Proc. Natl. Acad. Sci. U.S.A.* **103**, 11754–11759 (2006).
17. P. Fehlbaum, P. Bulet, S. Chernysh, J. P. Briand, J. P. Roussel, L. Letellier, C. Hetru, J. A. Hoffmann, Structure-activity analysis of thanatin, a 21-residue inducible insect defense peptide with sequence homology to frog skin antimicrobial peptides. *Proc. Natl. Acad. Sci. U.S.A.* **93**, 1221–1225 (1996).
18. I. A. Edwards, A. G. Elliott, A. M. Kavanagh, J. Zuegg, M. A. T. Blaskovich, M. A. Cooper, Contribution of amphipathicity and hydrophobicity to the antimicrobial activity and cytotoxicity of β-hairpin peptides. *ACS Infect. Dis.* **2**, 442–450 (2016).
19. Z. Hou, J. Lu, C. Fang, Y. Zhou, H. Bai, X. Zhang, X. Xue, Y. Chen, X. Luo, Underlying mechanism of in vivo and in vitro activity of C-terminal-amidated thanatin against clinical isolates of extended-spectrum β-lactamase-producing *Escherichia coli*. *J. Infect. Dis.* **203**, 273–282 (2011).
20. B. Ma, C. Niu, Y. Zhou, X. Xue, J. Meng, X. Luo, Z. Hou, The disulfide bond of the peptide thanatin is dispensible for its antimicrobial activity in vivo and in vitro. *Antimicrob. Agents Chemother.* **60**, 4283–4289 (2016).
21. Y. Shai, Mode of action of membrane active antimicrobial peptides. *Biopolymers* **66**, 236–248 (2002).
22. C.-F. Le, C.-M. Fang, S. D. Sekaran, Intracellular targeting mechanisms by antimicrobial peptides. *Antimicrob. Agents Chemother.* **61**, e02340-16 (2017).
23. P. Rassam, N. A. Copeland, O. Birkholz, C. Tóth, M. Chavent, A. L. Duncan, S. J. Cross, N. G. Housden, R. Kaminska, U. Seger, D. M. Quinn, T. J. Garrod, M. S. P. Sansom, J. Piehler, C. G. Baumann, C. Kleanthous, Supramolecular assemblies underpin turnover of outer membrane proteins in bacteria. *Nature* **523**, 333–336 (2015).
24. M. Urfer, J. Bogdanovic, F. Lo Monte, K. Moehle, K. Zerbe, U. Omasits, C. H. Ahrens, G. Pessi, L. Eberl, J. A. Robinson, A peptidomimetic antibiotic targets outer membrane proteins and disrupts selectively the outer membrane in *Escherichia coli*. *J. Biol. Chem.* **291**, 1921–1932 (2016).
25. N. Srinivas, P. Jetter, B. J. Ueberbacher, M. Werneburg, K. Zerbe, J. Steinmann, B. Van der Meijden, F. Bernardini, A. Lederer, R. L. A. Dias, P. E. Misson, H. Henze, J. Zumbrunn, F. O. Gombert, D. Obrecht, P. Hunziker, S. Schauer, U. Ziegler, A. Käch, L. Eberl, K. Riedel, S. J. DeMarco, J. A. Robinson, Peptidomimetic antibiotics target outer-membrane biogenesis in *Pseudomonas aeruginosa*. *Science* **327**, 1010–1013 (2010).
26. B. Van der Meijden, J. A. Robinson, Synthesis and application of photoproline - a photoactivatable derivative of proline. *ARKIVOC* **2011**, 130–136 (2011).
27. S.-S. Chng, M. Xue, R. A. Garner, H. Kadokura, D. Boyd, J. Beckwith, D. Kahne, Disulfide rearrangement triggered by translocon assembly controls lipopolysaccharide export. *Science* **337**, 1665–1668 (2012).
28. N. Ruiz, S.-S. Chng, A. Hiniker, D. Kahne, T. J. Silhavy, Nonconsecutive disulfide bond formation in an essential integral outer membrane protein. *Proc. Natl. Acad. Sci. U.S.A.* **107**, 12245–12250 (2010).
29. A. X. Tran, C. Dong, C. Whitfield, Structure and functional analysis of LptC, a conserved membrane protein involved in the lipopolysaccharide export pathway in *Escherichia coli*. *J. Biol. Chem.* **285**, 33529–33539 (2010).
30. K. M. Schultz, T. J. Lundquist, C. S. Klug, Lipopolysaccharide binding to the periplasmic protein LptA. *Protein Sci.* **26**, 1517–1523 (2017).
31. K. M. Schultz, J. B. Feix, C. S. Klug, Disruption of LptA oligomerization and affinity of the LptA–LptC interaction. *Protein Sci.* **22**, 1639–1645 (2013).
32. K. E. Park, S. H. Jang, J. Lee, S. A. Lee, Y. Kikuchi, Y. S. Seo, B. L. Lee, The roles of antimicrobial peptide, rip-thanatin, in the midgut of Riptortus pedestris. *Dev. Comp. Immunol.* **78**, 83–90 (2018).
33. M. Choi, C.-Y. Chang, T. Clough, D. Broudy, T. Killeen, B. MacLean, O. Vitek, MSstats: an R package for statistical analysis of quantitative mass spectrometry-based proteomic experiments. *Bioinformatics* **30**, 2524–2526 (2014).
34. M. Sattler, J. Schleucher, C. Griesinger, Heteronuclear multidimensional NMR experiments for the structure determination of proteins in solution employing pulsed field gradients. *Prog. Nucl. Magn. Reson. Spectrosc.* **34**, 93–158 (1999).
35. T. Yamazaki, J. D. Forman-Kay, L. E. Kay, Two-dimensional NMR experiments for correlating carbon-13.beta. and proton.delta./.epsilon. chemical shifts of aromatic residues in 13C-labeled proteins via scalar couplings. *J. Am. Chem. Soc.* **115**, 11054–11055 (1993).
36. Y. Shen, F. Delaglio, G. Cornilescu, A. Bax, *TALOS*+: A hybrid method for predicting protein backbone torsion angles from NMR chemical shifts. *J. Biomol. NMR* **44**, 213–223 (2009).
37. E. Michel, A. Plückthun, O. Zerbe, Peptide-guided assembly of repeat protein fragments. *Angew. Chem. Int. Ed.* **57**, 4576–4579 (2018).
38. C. Massif, S. Dautrey, A. Haefele, R. Ziessel, P.-Y. Renard, A. Romieu, New insights into water solubilization of fluorophores by post-synthetic "click" and Sonogashira reactions. *Org. Biomol. Chem.* **10**, 4330–4336 (2012).
39. M. L. Cunningham, B. P. Kwan, K. J. Nelson, D. C. Bensen, K. J. Shaw, Distinguishing on-target versus off-target activity in early antibacterial drug discovery using a macromolecular synthesis assay. *J. Biomol. Screen.* **18**, 1018–1026 (2013).
40. S.-S. Chng, N. Ruiz, G. Chimalakonda, T. Silhavy, D. Kahne, Characterization of the two-protein complex in *Escherichia coli* responsible for lipopolysaccharide assembly at the outer membrane. *Proc. Natl. Acad. Sci. U.S.A.* **107**, 5363–5368 (2010).
41. Z.-X. Wang, An exact mathematical expression for describing competitive binding of two different ligands to a protein molecule. *FEBS Lett.* **360**, 111–114 (1995).
42. B. J. Stockman, C. Dalvit, NMR screening techniques in drug discovery and drug design. *Prog. Nucl. Magn. Reson. Spectrosc.* **41**, 187–231 (2002).
43. P. Güntert, Automated NMR structure calculation with CYANA. *Methods Mol. Biol.* **278**, 353–378 (2004).
44. P. Güntert, L. Buchner, Combined automated NOE assignment and structure calculation with CYANA. *J. Biomol. NMR* **62**, 453–471 (2015).
45. N. Mandard, P. Sodano, H. Labbe, J.-M. Bonmatin, P. Bulet, C. Hetru, M. Ptak, F. Vovelle, Solution structure of thanatin, a potent bactericidal and fungicidal insect peptide, determined from proton two-dimensional nuclear magnetic resonance data. *Eur. J. Biochem.* **256**, 404–410 (1998).
46. C. D. Schwieters, J. Kuszewski, G. M. Clore, Using Xplor–NIH for NMR molecular structure determination. *Prog. Nucl. Magn. Reson. Spectrosc.* **48**, 47–62 (2006).

Acknowledgments: We thank M. Gwerder, the Center for Microscopy and Image Analysis at UZH, and the Functional Genomics Center Zurich for technical support. **Funding:** The following agencies are thanked for funding M.Mü. and B.W.: ETH (grant ETH-30 17-1) and Swiss National Science Foundation (grant 31003A_160259). J.A.R. was supported by the University of Zurich and the Swiss National Science Foundation (grant 205320_146381).
Author contributions: S.U.V., K.Z., M.U., M.Mo., and S.-Y.W. performed chemical and biochemical experiments. K.M. and O.Z. conceived and performed NMR studies. K.Z., A.V., G.P., and L.E. conceived and performed genetic analyses, and M.Mü. and B.W. conceived and performed MS-based proteomic studies. All authors contributed to the analysis and interpretation of results, and J.A.R. wrote the paper, which was seen and agreed by all other authors. **Competing interests:** The authors declare that they have no competing interests. **Data and materials availability:** All data needed to evaluate the conclusions in the paper are present in the paper and/or the Supplementary Materials. Additional data related to this paper may be requested from the authors. The PDB coordinates of the thanatin-$LptA_m$ structure will be available in the PDB database after publication under accession number 6GD5. Mass spectrometric data will be available at the ProteomeXchange Consortium (www.proteomexchange.org/) via the PRIDE partner repository (data set identifier: PXD010988). All NMR chemical shifts will be deposited in the BMRB database under ID 34261.

Submitted 23 May 2018
Accepted 16 October 2018
Published 14 November 2018
10.1126/sciadv.aau2634

Citation: S. U. Vetterli, K. Zerbe, M. Müller, M. Urfer, M. Mondal, S.-Y. Wang, K. Moehle, O. Zerbe, A. Vitale, G. Pessi, L. Eberl, B. Wollscheid, J. A. Robinson, Thanatin targets the intermembrane protein complex required for lipopolysaccharide transport in *Escherichia coli*. *Sci. Adv.* **4**, eaau2634 (2018).

Science Advances

Thanatin targets the intermembrane protein complex required for lipopolysaccharide transport in *Escherichia coli*

Stefan U. Vetterli, Katja Zerbe, Maik Müller, Matthias Urfer, Milon Mondal, Shuang-Yan Wang, Kerstin Moehle, Oliver Zerbe, Alessandra Vitale, Gabriella Pessi, Leo Eberl, Bernd Wollscheid and John A. Robinson

Sci Adv **4** (11), eaau2634.
DOI: 10.1126/sciadv.aau2634